

Turbo Receiver Design for Coded Differential PSK in Bursty Impulsive Noise Channels

Chin-Hung Chen, *Student Member, IEEE*, Boris Karanov, *Member, IEEE*,
Wim van Houtum, *Senior Member, IEEE*, Yan Wu, and Alex Alvarado, *Senior Member, IEEE*

Abstract—It has been recognized that the impulsive noise (IN) generated by power devices poses significant challenges to wireless receivers. In this paper, we comprehensively assess the achievable information rate (AIR) for the well-established Markov-Middleton IN model with a phase-shift keying (PSK) input sequence across various channel conditions, including matched and mismatched decoding scenarios. Upon determining information-theoretic bounds, we propose an optimal turbo-DPSK-IN receiver design based on a commonly used commercial transmission setup consisting of a convolutional encoder, bit-level interleaver, and a differential PSK (DPSK) symbol mapper. We show that by incorporating the differential decoder into the maximum a-posteriori-based (MAP) IN detector, we can significantly enhance the receiver performance with a 4.5 dB gain compared to the conventional MAP-based PSK-IN receiver and a gap of around 1 dB to the theoretical bounds. We also propose a suboptimal separate receiver design that can be implemented with half the complexity of the joint design and near-optimal performance. We have evaluated the performance of the proposed receiver designs through extensive simulations, demonstrating their effectiveness in real-world scenarios with limited interleaver depth and mismatched state implementation.

Index Terms—Achievable information rate, convolutional codes, differential modulation, impulsive noise, Markov channels, symbol detection, turbo decoding.

I. INTRODUCTION

ELECTROMAGNETIC interference (EMI) generated by power devices such as switching gears, power lines, and DC-DC converters present significant challenges to conventional receivers designed for the additive white Gaussian noise (AWGN). Measurements have shown that electronic components in electric vehicles (EVs) [1]–[4] and power substations [5], [6] emit EMI that can be detected by high-sensitivity receivers. Specifically, the impulsive nature of this interference has been demonstrated to have a crucial impact on powerline communications [7], [8], digital broadcasting systems [9], [10], and wireless communication receivers within power substations [11]–[13].

Manuscript received xx, xxxx; revised xx, xxxx.

C.-H. Chen, W. van Houtum, and A. Alvarado are with the Information and Communication Theory (ICT) Lab, Electrical Engineering Department, Eindhoven University of Technology, 5600MB Eindhoven, The Netherlands. W. van Houtum is also with NXP Semiconductors, High Tech Campus 60, 5656AE Eindhoven, The Netherlands. (e-mails: c.h.chen@tue.nl; w.j.v.houtum@tue.nl; a.alvarado@tue.nl).

B. Karanov was with the ICT Lab, and is now with the Communications Engineering Lab (CEL), Karlsruhe Institute of Technology, 76187 Karlsruhe, Germany (e-mail: boris.karanov@kit.edu).

Y. Wu is with NXP Semiconductors, High Tech Campus 60, 5656AE Eindhoven, The Netherlands. (e-mail: yan.wu_2@nxp.com).

Conventional clipping [14] and blanking [15] detectors for IN mitigation are widely adopted due to their simple implementation and the low computational complexity. However, their performance is far from optimal especially in severe IN channel conditions [23]. To design robust receivers for channels impaired by IN, it is essential to obtain their statistical properties, and therefore an appropriate IN model is necessary. One of the well-known IN models is the Middleton Class A model [16], [17], which is characterized by a Poisson-distributed IN with a tractable probability density function that can be specified by only three parameters. Despite its straightforward representation, this model does not adequately describe the bursty behavior of the IN. Therefore, the hidden-Markov model (HMM) has been adopted for IN modeling [8], [18], [19] to address the correlation between impulsive samples. In [18], a two-state Markov-Gaussian model was proposed, where comprehensive achievable information rate (AIR) analysis was presented. In [19], the authors combined the HMM process with the Middleton Class A model and proposed the Markov-Middleton model. In our earlier study [4], we found that a Markov-Middleton model with finite IN states effectively represents the EV-induced interference in practice. However, to the best of our knowledge, an information-theoretical analysis of this model has not been thoroughly investigated; therefore, one of the goals of this paper is to fill this gap by conducting a detailed AIR analysis under various channel conditions for both matched and mismatched decoding scenarios.

Optimal IN detector design takes into account the statistical properties of the noise and computes the maximum a-posteriori (MAP) solutions to handle the IN and recover the transmitted symbols. In [19]–[23], several optimal MAP-based IN detectors have been derived for different IN models. To further enhance the receiver performance, powerful coding systems in combination with the IN detector have been extensively investigated to approach the AIR for the underlying channel model [18], [19], [23]–[28]. Receivers for these schemes take the soft information provided by the MAP-based IN detector and pass it to the powerful decoding algorithms, such as low-density parity-check (LDPC) codes [18], [19], [23], [24], convolutional codes [25], [26] and turbo-like codes [27], [28]. However, previous studies have primarily focused on a basic binary phase-shift keying (BPSK) modulation scheme, mainly addressing the design of its corresponding IN detector and decoder. There has been limited investigation into more complex modulation schemes used in real-world transmission formats for IN receivers.

In wireless communication standards, a differential mapper, where the information is encoded in the phase difference between successive symbols, is commonly used to mitigate the effects of phase ambiguity and for noncoherent detection. For example, digital audio broadcasting, terrestrial-digital multimedia broadcasting, and WiFi IEEE 802.11g use the combination of a convolutional encoder and differential PSK (DPSK) symbol mapper. Although initially designed for non-coherent detection, research has demonstrated that a coherent DPSK demapper can be constructed, wherein the soft information output can be computed using the MAP rule [29]. Since then, turbo-DPSK systems, which combine a MAP DPSK demapper with a MAP decoder, have been explored in a broad range of literature, see [30]–[32] and references therein. The recursive nature of the DPSK modulator increases the time diversity of a serial turbo-like receiver structure. As a result, a turbo-DPSK system achieves significant performance gains compared to a simple PSK receiver, as reported in [33].

In this paper, we propose to combine a simple differential demapper with the MAP IN detector, thus forming a MAP-based joint DPSK-IN demapper, which can be implemented with the same complexity as a conventional PSK-IN demapper. We further construct a turbo-DPSK-IN receiver structure, which outperforms its MAP-based PSK-IN counterpart significantly. This paper starts with an information-theoretical analysis of the Markov-Middleton channel and then performs turbo receiver designs to approach the estimated theoretical bounds. The contribution of this paper are four: (a) We provide a unified HMM representation for deriving AIR, MAP detector/demapper/decoder, and iterative decoding metrics through modified branch metrics. This general representation facilitates a streamlined analysis, reveals the underlying commonalities among different algorithms, and demonstrates that they can be systematically constructed under a similar forward-backward framework. (b) We extend the AIR analysis in [18] to adapt it to a finite-state Markov-Middleton channel with a PSK input sequences. Our comprehensive analysis covers both matched and mismatched decoding scenarios, providing an indication for receiver parameter selections. (c) We propose a novel turbo-DPSK-IN receiver design that approaches the theoretical bounds of the Markov-Middleton channel within around 1 dB gap, and we show that it can achieve a significant performance gain compared to the conventional PSK-IN receiver proposed in [18], [19]. The ultimate performance of the proposed receiver with perfect likelihood input is also presented, and (d) we further propose a suboptimal turbo-DPSK-IN receiver design that can be implemented with half the complexity of the optimal joint design with near-optimal performance. The proposed receiver with limited interleaver depth and a mismatched state implementation are also investigated and discussed.

The remainder of this paper is organized as follows: Sec. II presents the general structure and inference algorithm of HMMs. Sec. III reviews the Markov-Middleton IN channel and its HMM representation. Sec. IV illustrates the computation of the simulation-based AIR for the considered IN channel with a PSK input sequence. Sec. V details the proposed communication system and the design methodology

for the optimal joint and suboptimal separate turbo-DPSK-IN receivers. Sec. VI presents the simulation results for both AIR and the proposed receiver performance, and finally, Sec. VII concludes this paper.

II. HIDDEN MARKOV MODEL AND ITS EFFICIENT INFERENCE ALGORITHM

This section provides a general overview of the structure and statistical representation of HMMs. Additionally, we present the utilization of the forward-backward algorithm to compute joint probabilities of observations and latent variables. An HMM structure will be used to describe the Markov-Middleton IN channel in Sec. III, and the inference algorithm presented in this section will later be applied to AIR computation in Sec. IV, while the application to symbol detection, differential demapping, and convolutional decoding based on the MAP rule will be provided in Sec. V.

An HMM is a statistical model that captures the temporal behavior of a sequence of latent variables (states) from a Markov process via a sequence of state-dependent observable variables (observations). In particular, the model represents the joint distribution of the observed sequence $\mathbf{y}_1^T = (y_1, y_2, \dots, y_T)$ and the corresponding state sequence $\mathbf{s}_1^T = (s_1, s_2, \dots, s_T)$ as

$$p(\mathbf{s}_1^T, \mathbf{y}_1^T) = \prod_{t=1}^T p(s_t | s_{t-1}) p(y_t | s_t), \quad (1)$$

where at $t = 1$, the transition probability $p(s_1 | s_0)$ is defined as the initial state probability $p(s_1)$.¹ Here, s_t denotes the actual state realization at time t , which is drawn from a time-invariant finite-state set

$$s_t \in \mathcal{S} \triangleq \{0, 1, \dots, |\mathcal{S}| - 1\}, \quad (2)$$

where $|\mathcal{S}| = N$ is the size of the state space. This paper assumes that the state transition matrix is stationary, with each element representing the probability $p(s_t = j | s_{t-1} = i)$ of moving from state i at time $t-1$ to state j at time t . The second parameter on the right-hand side of (1) is the observation likelihood $p(y_t | s_t = j)$, which describes the probability of an observation being generated from a state j at time t . A general representation of the structure of an HMM is shown in Fig. 1.

The Markovian structure of an HMM allows an efficient inference of the hidden states through the well-known Bahl-Cocke-Jelinek-Raviv (BCJR) algorithm [35]. Specifically, the inference problem aims at calculating the posterior belief of a latent state s_t at a specific time instant given the full sequence of observations as

$$p(s_t | \mathbf{y}_1^T) \propto p(s_t, \mathbf{y}_1^T) = \sum_{s_{t-1} \in \mathcal{S}} p(s_t, s_{t-1}, \mathbf{y}_1^T). \quad (3)$$

The right-most side of (3) represents the joint distribution of the state pairs (s_t, s_{t-1}) at a specific time t and the whole

¹Throughout this paper, we use lowercase letters to represent a scalar with subscripts indicating a specific time instant and boldface letters to denote a sequence, with subscripts and superscripts denoting the start and end of the sequence.

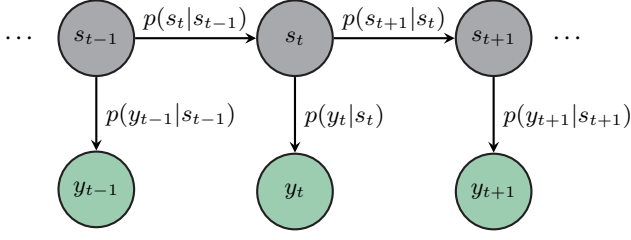


Fig. 1. Structure of a hidden Markov model representation in (1) showing the factorization and conditional independencies implied by the model.

received sequence \mathbf{y}_1^T . We can further factorize the joint probability as follows

$$p(s_t, s_{t-1}, \mathbf{y}_1^T) = p(s_t, s_{t-1}, \mathbf{y}_{t+1}^T, y_t, \mathbf{y}_1^{t-1}) \quad (4)$$

$$= p(\mathbf{y}_{t+1}^T | s_t, s_{t-1}, y_t, \mathbf{y}_1^{t-1}) \quad (5)$$

$$\begin{aligned} & \cdot p(y_t, s_t | s_{t-1}, \mathbf{y}_1^{t-1}) \cdot p(s_{t-1}, \mathbf{y}_1^{t-1}) \\ & = \underbrace{p(\mathbf{y}_{t+1}^T | s_t)}_{\beta(s_t)} \cdot \underbrace{p(y_t, s_t | s_{t-1})}_{\gamma(s_t, s_{t-1})} \cdot \underbrace{p(s_{t-1}, \mathbf{y}_1^{t-1})}_{\alpha(s_{t-1})}, \end{aligned} \quad (6)$$

where in (4), we separate the observation sequence into past time sequence \mathbf{y}_1^{t-1} , current time step y_t , and the future time sequence \mathbf{y}_{t+1}^T . From (4) to (5) Bayes' rule is used. The derivation of (6) from (5) is based on the Markovian conditional independencies implied by the graph in Fig. 1. Let $\alpha(s_{t-1})$, $\beta(s_t)$, and $\gamma(s_t, s_{t-1})$ represent $p(s_{t-1}, \mathbf{y}_1^{t-1})$, $p(\mathbf{y}_{t+1}^T | s_t)$, and $p(y_t, s_t | s_{t-1})$, respectively, corresponding to forward recursion, backward recursion, and branch metrics in (6).

Using Bayes' rule and Markovian property, the branch metric γ can be further derived as

$$\gamma(s_t, s_{t-1}) \triangleq p(y_t, s_t | s_{t-1}) = p(y_t | s_t) \cdot p(s_t | s_{t-1}) \quad (7)$$

which can be seen as the multiplication of the observation likelihood and the state transition probability. The forward recursion representation of α can be derived as

$$\alpha(s_t) \triangleq p(s_t, \mathbf{y}_1^t) = \sum_{s_{t-1} \in \mathcal{S}} p(s_t, s_{t-1}, y_t, \mathbf{y}_1^{t-1}) \quad (8)$$

$$= \sum_{s_{t-1} \in \mathcal{S}} p(y_t, s_t | s_{t-1}) \cdot p(s_{t-1}, \mathbf{y}_1^{t-1}) \quad (9)$$

$$= \sum_{s_{t-1} \in \mathcal{S}} \gamma(s_t, s_{t-1}) \cdot \alpha(s_{t-1}), \quad (10)$$

where in (8) the law of total probability is applied, and from (8) to (9) Bayes' rule and the Markovian property are used. Following a similar approach, we can represent the backward recursion β as

$$\begin{aligned} \beta(s_{t-1}) & \triangleq p(\mathbf{y}_t^T | s_{t-1}) = \sum_{s_t \in \mathcal{S}} p(s_t, \mathbf{y}_{t+1}^T, y_t | s_{t-1}) \\ & = \sum_{s_t \in \mathcal{S}} p(\mathbf{y}_{t+1}^T | s_t) \cdot p(y_t, s_t | s_{t-1}) \\ & = \sum_{s_t \in \mathcal{S}} \beta(s_t) \cdot \gamma(s_t, s_{t-1}). \end{aligned} \quad (11)$$

The forward-backward computation (3)–(11) of the posterior belief comprises the conventional BCJR algorithm. In this paper, we will examine several adaptations of this algorithm, each utilizing the same forward-backward framework but with modifications to the branch metrics γ that are tailored to specific applications.

III. MARKOV-MIDDLETON IMPULSIVE NOISE MODEL

In this section, we summarize the Markov-Middleton model, initially developed for powerline communications [19], which captures the statistical behavior of bursty IN by combining the conventional Middleton Class A model [16] with an HMM. The integration of HMM introduces memory between noise samples, with state transition probabilities characterizing the correlation between consecutive bursts.

The Markov-Middleton model is characterized by four parameters: the background noise (BN) variance σ_0^2 , the impulsive index A , which quantifies the probability of impulsive (non-BN) events, the impulsive-to-background noise power ratio Λ , which determines the intensity of IN compared to BN, and the noise correlation parameter r , which describes the correlation between consecutive noise samples. The noise realizations generated by the Markov-Middleton model for different parameters are depicted in Figs. 2a–2d, and will be further explained in the following.

The statistical properties of the impulsive noise samples n_t are completely determined by the channel noise state realization at time t , which is defined as

$$w_t \in \mathcal{W} \triangleq \{0, 1, \dots, |\mathcal{W}| - 1\}, \quad (12)$$

where $w_t = 0$ represents the BN state and $|\mathcal{W}| = W$ is the total number of channel noise states. The probability density function (PDF) of n_t conditioned on a specific noise state $w_t = j$ can be written as

$$p(n_t | w_t = j) = \frac{1}{\sqrt{2\pi\sigma_j^2}} \exp\left(-\frac{n_t^2}{2\sigma_j^2}\right), \quad (13)$$

where σ_j^2 is the variance of the noise sample n_t being at a specific state $w_t = j$.

In the original Middleton Class A model [16], the number of noise states is assumed to be infinity ($W \rightarrow \infty$). Therefore, the generic PDF of the Middleton Class A noise sample can be written as the expectation over all possible states as

$$\begin{aligned} p(n_t) & = \sum_{j=0}^{\infty} p(w_t = j) \cdot p(n_t | w_t = j) \\ & = \sum_{j=0}^{\infty} \frac{p(w_t = j)}{\sqrt{2\pi\sigma_j^2}} \exp\left(-\frac{n_t^2}{2\sigma_j^2}\right), \end{aligned} \quad (14)$$

where

$$p(w_t = j) = e^{-A} A^j / j! \quad (15)$$

represents the prior probability of being at a specific noise state. From (15), we can observe that when $j = 0$, the probability of being at BN state $w_t = 0$ is $p_B = p(w_t = 0) = e^{-A}$ and the probability of being at any of the impulsive states

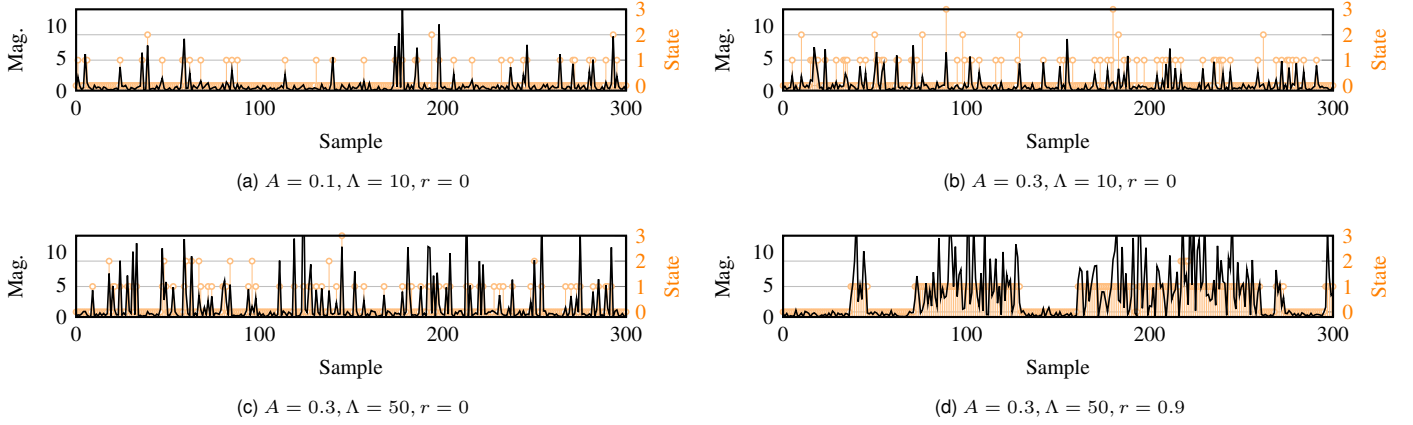


Fig. 2. Noise realization from a 4-state Markov-Middleton impulsive noise model with a background noise variance $\sigma_0^2 = 1$ for impulsive index $A = 0.1$ and $A = 0.3$, impulsive-to-background noise power ratio $\Lambda = 10$ and $\Lambda = 50$, and correlation parameters $r = 0$ and $r = 0.9$. The orange vertical bar denotes the index j of the state realizations $w_t = j$ for generating the corresponding noise samples.

$j > 0$ is $p_I = 1 - e^{-A}$. In other words, a larger impulsive index A results in a larger p_I , and thus, more noises with large variance (σ_j^2 , $j > 0$) are generated in a noise sequence \mathbf{n}_I^T . As shown in Figs. 2a and 2b, when the impulsive index A is increased from 0.1 to 0.3, the number of noise in IN states ($j > 0$) increases.

As illustrated in (15), the probability of being in the j -th noise state decreases as j increases. Therefore, it is sufficient to use a truncated Middleton Class A model with a finite number of states W to represent the IN channel with

$$p(n_t) = \sum_{j=0}^{W-1} \frac{p'(w_t = j)}{\sqrt{2\pi\sigma_j^2}} \exp\left(-\frac{n_t^2}{2\sigma_j^2}\right), \quad (16)$$

where the probability of being in state j is now written as

$$p'(w_t = j) = \frac{p(w_t = j)}{\sum_{i=0}^{W-1} p(w_t = i)}. \quad (17)$$

The denominator in (17) is a normalization factor to ensure the total probability equals 1.

The noise variance in (16) is defined as

$$\sigma_j^2 = \left(1 + \frac{j\Lambda}{A}\right) \sigma_0^2, \quad (18)$$

where

$$\Lambda = \sigma_I^2 / \sigma_B^2 \quad (19)$$

is the impulsive-to-background average noise power ratio.² The average BN power is $\sigma_B^2 = p'(w_t = 0)\sigma_0^2$ and the average IN power σ_I^2 can be written as

$$\sigma_I^2 = \sum_{j=1}^{W-1} p'(w_t = j)\sigma_j^2.$$

From (19), we can see that as the impulsive-to-background noise ratio Λ increases, the difference between the IN power and the BN power increases. This is clearly shown by comparing the noise realizations (black lines) in Figs. 2b and 2c.

²In the original paper [16], the power ratio is defined as $\Gamma = \sigma_B^2 / \sigma_I^2$.

To describe the burstiness (memory) of the noise observed in practice, the Markov-Middleton model [19] introduces a parameter $r \in [0, 1]$ to establish a correlation between consecutive noise samples. Specifically, the state transition matrix of the Markov-Middleton noise model is constructed as

$$P_{ij} \triangleq p(w_t = j | w_{t-1} = i) = \begin{cases} r + (1-r) \cdot p'(w_t = j), & i = j \\ (1-r) \cdot p'(w_t = j), & \text{otherwise.} \end{cases} \quad (20)$$

From (20), we can see that the larger the correlation parameter r , the more likely the following noise sample will stay in the same state. Namely, the bursty behavior is more prominent. In Fig. 2d, the noise samples exhibit strong correlations ($r = 0.9$), where the noise tends to remain in the same state (vertical orange bars) for consecutive samples. In contrast, in Figs. 2a–2c, the noise samples are randomly chosen from $w_t \in \mathcal{W}$ with probability $p'(w_t = j)$ defined in (17). Note that when $r = 0$, the Markov-Middleton model is reduced to a truncated memoryless Middleton Class A channel.

IV. ACHIEVABLE INFORMATION RATE

This section presents an information-theoretical analysis for transmission over channels with IN following the Markov-Middleton model introduced in Sec. III. This is an essential reference for practical receiver design operating in specific channel conditions. We use a simulation-based method to calculate the AIR between the PSK-modulated input sequence \mathbf{x}_1^T and the channel output sequence \mathbf{y}_1^T with an input-output relationship defined as

$$y_t = x_t + n_t, \quad (21)$$

where

$$x_t \in \mathcal{X} = \{e^{j2\pi i/M} \mid i = 0, 1, \dots, M-1\} \quad (22)$$

denotes the transmitted M -ary PSK symbol and n_t follows the Markov-Middleton noise model described in Sec. III, which is drawn from the distribution defined in (16). The computation of AIR for channels with memory is explained in detail in [34],

and its application to a two-state Markov-Gaussian channel is described in [18]. The algorithm and the computation steps are briefly summarized as follows.

An AIR is the number of information bits that can be reliably transmitted and decoded, with an arbitrarily low error probability per channel use, for a specific modulation format. Specifically, the AIR we consider in this work is the mutual information $I(\mathbf{X}; \mathbf{Y})$ between the discrete input random process \mathbf{X} and the continuous output random process \mathbf{Y} , which can be estimated via

$$I(\mathbf{X}; \mathbf{Y}) \approx \hat{I}(\mathbf{X}; \mathbf{Y}) = \frac{1}{T} \log p(\mathbf{y}_1^T | \mathbf{x}_1^T) - \frac{1}{T} \log p(\mathbf{y}_1^T) \quad (23)$$

with a very long sequence T . To calculate (23) for channels with memory, [34] introduces a simulation-based computation through a sum-product algorithm with the help of an auxiliary state process. In this paper, we define the auxiliary state realization for a PSK-modulated symbol over a Markov-Middleton IN channel as

$$a_t = f(x_t \in \mathcal{X}, w_t \in \mathcal{W}) \in \mathcal{A} \triangleq \{0, 1, \dots, |\mathcal{A}| - 1\}, \quad (24)$$

where $f: \mathcal{X} \times \mathcal{W} \rightarrow \mathcal{A}$ maps each pair (x_t, w_t) in the product space $\mathcal{X} \times \mathcal{W}$ into a unique state in \mathcal{A} . The size of the auxiliary state space is thus $|\mathcal{A}| = |\mathcal{X}| \times |\mathcal{W}| = M \times W$. In Fig. 3a, we show an example of the trellis section and the auxiliary state for a QPSK transmission (i.e., $M = 4$) over a 2-state (i.e., $W = 2$) Markov-Middleton channel.

The transition probability of the auxiliary states considers the prior PSK symbol probability $p(x_t)$ and the noise state transition matrix defined in (20), which can be expressed as

$$p(a_t | a_{t-1}) = P_{ij} \cdot p(x_t), \quad w_t = j, w_{t-1} = i. \quad (25)$$

The channel likelihood function concerning the auxiliary states (24) can be written as

$$p(y_t | a_t) = \frac{1}{\sqrt{2\pi\sigma_j^2}} \exp\left(-\frac{(y_t - x_t)^2}{2\sigma_j^2}\right), \quad w_t = j. \quad (26)$$

After determining the auxiliary states with their statistical representation (25) and (26), the PDF of the channel output sequence $p(\mathbf{y}_1^T)$ can be calculated via

$$p(\mathbf{y}_1^T) = \sum_{a_T \in \mathcal{A}} p(a_T, \mathbf{y}_1^T) = \sum_{a_T \in \mathcal{A}} \alpha(a_T), \quad (27)$$

using forward recursion (8)–(10), with a branch metric

$$\gamma_a(a_t, a_{t-1}) \triangleq p(y_t | a_t) \cdot p(a_t | a_{t-1}). \quad (28)$$

To compute the PDF of the channel output sequence conditioned on the knowledge of the transmitted symbol sequence $p(\mathbf{y}_1^T | \mathbf{x}_1^T)$, we write

$$p(\mathbf{y}_1^T | \mathbf{x}_1^T) = \frac{p(\mathbf{y}_1^T, \mathbf{x}_1^T)}{p(\mathbf{x}_1^T)} = \frac{\sum_{a_T \in \mathcal{A}} p(a_T, \mathbf{y}_1^T, \mathbf{x}_1^T)}{p(\mathbf{x}_1^T)} \quad (29)$$

with the help of the auxiliary state. The computation of the joint probability $p(a_T, \mathbf{y}_1^T, \mathbf{x}_1^T)$ can be carried out efficiently

using the forward recursion (8)–(10) with a modified branch matrix defined as

$$\begin{aligned} \gamma_{a,x}(a_t, a_{t-1}) &\triangleq p(y_t, x_t, a_t | a_{t-1}) \\ &= p(y_t | x_t, a_t, a_{t-1}) \cdot p(a_t | a_{t-1}, x_t) \cdot p(x_t | a_{t-1}) \\ &= p(y_t | a_t) \cdot p(a_t | a_{t-1}, x_t) \cdot p(x_t), \end{aligned} \quad (30)$$

where the transition probability conditioned to the knowledge of transmitted symbols is written as

$$\begin{aligned} p(a_t | a_{t-1}, x_t = m \in \mathcal{X}) &= \begin{cases} P_{ij}, & x_t = m, w_t = j, w_{t-1} = i, \\ 0, & x_t \neq m, \end{cases} \end{aligned} \quad (31)$$

where we use m to denote a specific PSK symbol element in \mathcal{X} . Given (27) and (29), the estimated AIR, represented by $\hat{I}(\mathbf{X}; \mathbf{Y})$ can be computed via (23).

V. SYSTEM DESIGN

In Fig. 4, we show the overall structure and components of the transmission system over a Markov-Middleton IN channel considered in this paper. This section will first introduce the bit-interleaved convolutional-coded DPSK transmitter and then detail the design methodology for the corresponding turbo-DPSK-IN receiver.

A. Bit-Interleaved Convolutional-Coded DPSK Transmitter

On the transmitter side, a serially concatenated bit-interleaved coded modulation is constructed for transmission. In this system, a rate R convolutional encoder with L -stage shift register takes as input the information bit sequence \mathbf{b}_1^K and generates coded bit sequence output $\mathbf{c}_1^{K/R}$, where $b_k, c_k \in \{0, 1\}$, based on a certain generator constraint. A bit-level interleaver (II) is used to permute the convolutional encoder output, where the interleaved coded bit sequence is represented as $\mathbf{d}_1^{K/R}$. The bit-interleaver is designed to transform burst errors into single-bit errors that ensure that errors are distributed to maximize error correction capability, which is essential for turbo decoding. After the interleaver, a symbol sequence \mathbf{x}_1^T is formed by a memoryless PSK symbol mapper, which maps a number of binary coded bits to a PSK symbol with the symbol time index denoted by the letter t . Finally, a differential symbol encoder modulates the incoming PSK symbols and generates the differentially encoded PSK (DPSK) symbol sequence \mathbf{z}_0^T by

$$z_t = x_t \cdot z_{t-1}, \quad (32)$$

where we define $z_0 = 1$ and $z_t \in \mathcal{X}$. This extra differential modulation leads to a channel input-output relationship of

$$y_t = x_t \cdot z_{t-1} + n_t = z_t + n_t. \quad (33)$$

Differential encoders are used in various wireless communication standards. One of the most significant advantages of a differential encoder is that it avoids the need for the receiver to have an exact phase reference, as the information is encoded in the phase difference of consecutive symbols. In this paper, we treat the differential encoder as a rate one convolutional

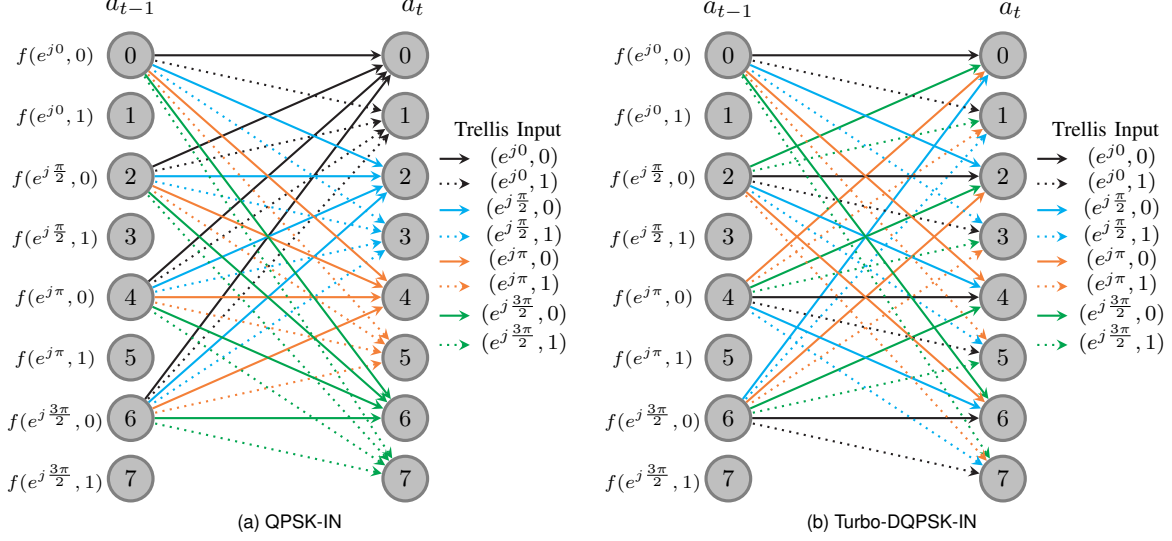


Fig. 3. Trellis sections of an impulsive noise detector with a 2-state Markov-Middleton model for (a) QPSK and (b) DQPSK transmissions, respectively. For clarity, we only show the state transitions from states 0, 2, 4, and 6.

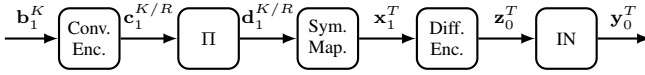
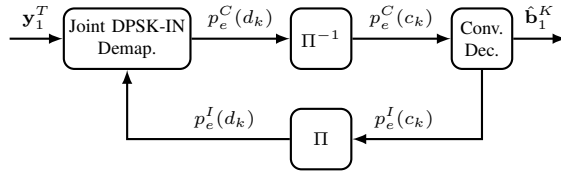
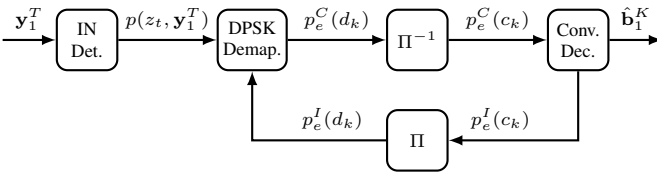


Fig. 4. Block diagram of a convolutional-coded bit-interleaved DPSK transmission over an impulsive noise channel



(a) Joint receiver design



(b) Separate receiver design

Fig. 5. Block diagrams of (a) optimal joint and (b) the suboptimal separate turbo-DPSK-IN receiver designs.

code [30], [33] and thus create a serial-like turbo structure with the convolutional encoder. Its recursive structure largely enhances the time diversity in the serial turbo receiver design, leading to significant performance improvement compared to memoryless PSK modulation schemes [31], [32]. This study assumes a coherent detection scenario with a known symbol phase. As a result, we will ignore the reference symbols z_0 and y_0 in the subsequent analysis.

B. Optimal Joint Turbo-DPSK-IN Receiver

1) *MAP DPSK-IN demapper*: In the joint detector-demapper design, we construct a super-trellis where the structure of the Markov-Middleton IN detector and the DPSK demapper are considered jointly. We define the state realization of the joint super-trellis as

$$\dot{a}_t = f(z_t \in \mathcal{X}, w_t \in \mathcal{W}) \in \mathcal{A}, \quad (34)$$

which is drawn from the same state space as a_t in (24) and has a similar form of transition probability

$$p(\dot{a}_t | \dot{a}_{t-1}) = P_{ij} \cdot p(x_t), \quad w_t = j, w_{t-1} = i. \quad (35)$$

However, instead of the PSK symbol x_t , the state \dot{a}_t is now associated with the differentially encoded symbol z_t with a transition driven by x_t . The transition of the joint super-trellis section for a DQPSK modulation with a 2-state Markov-Middleton model is visualized in Fig. 3b. We can now define the branch metric

$$\begin{aligned} \gamma_{\dot{a}}(\dot{a}_t, \dot{a}_{t-1}) &\triangleq p(y_t | \dot{a}_t) \cdot p(\dot{a}_t | \dot{a}_{t-1}) \\ &= p(y_t | a_t) \cdot p(\dot{a}_t | \dot{a}_{t-1}). \end{aligned} \quad (36)$$

Given the likelihood function (26) and transition probability (35) for computing the branch metric (36), the joint probability $p(\dot{a}_t, \dot{a}_{t-1}, \mathbf{y}_1^T)$ of the joint DPSK-IN detector-demapper is computed via (4)–(11). A MAP-based soft-output detection is then performed through

$$p(x_t, \mathbf{y}_1^T) = \sum_{(\dot{a}_{t-1} \rightarrow \dot{a}_t) : x_t} p(\dot{a}_t, \dot{a}_{t-1}, \mathbf{y}_1^T).$$

where $(\dot{a}_{t-1} \rightarrow \dot{a}_t) : x_t$ denotes all the state transitions $(\dot{a}_{t-1} \rightarrow \dot{a}_t)$ that is driven by the input symbol x_t .

2) *Iterative Turbo Decoder*: To perform bit deinterleaving, we need to convert the symbol probability to bit probability as

$$p(d_k, \mathbf{y}_1^T) = \Phi^{-1}[p(x_t, \mathbf{y}_1^T)] \quad (37)$$

and

$$p_e^I(d_k) = \Phi^{-1}[p_e^I(x_t)],$$

where Φ^{-1} denotes the inverse symbol mapping function that converts the probability of the PSK symbol x_t back to the probability of the corresponding bit d_k .

One essential part of the turbo decoding principle is to pass only the extrinsic information to each MAP decoder (demapper) block. Extrinsic information refers to the information provided by one decoder (demapper) about one specific bit (symbol), excluding the information directly used to derive it. In other words, it represents new information that can help the other decoder (demapper) refine its estimates. Here, we define the extrinsic likelihood information from the joint DPSK-IN demapper as the joint probability $p(d_k, \mathbf{y}_1^T)$ divided by the prior information regarding d_k as

$$p_e^C(d_k) \triangleq \frac{p(d_k, \mathbf{y}_1^T)}{p_e^I(d_k)}.$$

After performing the bit-deinterleaving, we can derive the extrinsic likelihood information of the coded bits as

$$p_e^C(c_k) = \Pi^{-1}[p_e^C(d_k)],$$

which is then fed to the convolutional decoder, whose state realization is defined as

$$\begin{aligned} g_k &= f(b_k, b_{k-1}, \dots, b_{k-L-1} \in \mathcal{U}^L) \\ &\in \mathcal{G} \triangleq \{0, 1, \dots, 2^L - 1\}, \end{aligned}$$

where $f : \mathcal{U}^L \rightarrow \mathcal{G}$ maps \mathcal{U}^L to distinct states in \mathcal{G} . The modified branch metric for the convolutional decoder is then written as

$$\gamma_g(g_k, g_{k-1}) \triangleq p_e^C(c_k) \cdot p(b_k), \quad (g_{k-1} \rightarrow g_k) : b_k. \quad (38)$$

The extrinsic likelihood information $p_e^C(c_k)$ produced by the DPSK demapper acts as the convolutional decoder's likelihood information, and $p(b_k) = 1/2$ is the prior bit probability. Again, we compute the joint probability $p(g_k, g_{k-1}, \mathbf{y}_1^T)$ via (4)–(11) using (38) and obtain the joint probability of the information bit as

$$p(b_k, \mathbf{y}_1^T) = \sum_{(g_{k-1} \rightarrow g_k) : b_k} p(g_k, g_{k-1}, \mathbf{y}_1^T),$$

and the joint probability of the coded bit as

$$p(c_k, \mathbf{y}_1^T) = \sum_{(g_{k-1} \rightarrow g_k) : c_k} p(g_k, g_{k-1}, \mathbf{y}_1^T).$$

To compute the extrinsic prior information produced by the convolutional decoder, we divide the joint probability $p(c_k, \mathbf{y}_1^T)$ by the likelihood function $p_e^C(c_k)$ used for deriving it as

$$p_e^I(c_k) \triangleq \frac{p(c_k, \mathbf{y}_1^T)}{p_e^C(c_k)}.$$

After the bit interleaver

$$p_e^I(d_k) = \Pi[p_e^I(c_k)],$$

we can derive the extrinsic prior information of the PSK symbol via bit-to-symbol mapping

$$p_e^I(x_t) = \Phi[p_e^I(d_k)].$$

The extrinsic symbol information $p_e^I(x_t)$ generated by the convolutional decoder is then fed back as the prior information in (41) of the joint DPSK-IN demapper for the next turbo iteration.

C. Suboptimal Separate Turbo-DPSK-IN Receiver

While the joint design delivers the optimal MAP solution by iteratively updating the extrinsic information for both the IN detector and DE demapper simultaneously, the computational complexity increases significantly with the number of turbo iterations. Therefore, we introduce in this section a suboptimal design that separates the IN detector from the turbo-DPSK demapper-decoder to reduce the operational complexity.

1) *MAP IN Detector*: The states of the standalone MAP-based IN detector are defined as in (24), and a trellis section example is shown in Fig. 3a. Given the transition probability (25), likelihood function (26), and the branch metric (28), the joint probability $p(a_t, a_{t-1}, \mathbf{y}_1^T)$ of the IN detector is computed via (4)–(11). A MAP-based soft-output detection is then performed through

$$p(z_t, \mathbf{y}_1^T) = \sum_{(a_{t-1} \rightarrow a_t) : z_t} p(a_t, a_{t-1}, \mathbf{y}_1^T). \quad (39)$$

where $(a_{t-1} \rightarrow a_t) : z_t$ denotes all the state transitions $(a_{t-1} \rightarrow a_t)$ that is driven by the input differentially encoded symbol z_t .

2) *MAP DE Demapper*: The joint probability (39) generated from the IN detector is used as a soft input, representing the channel information, to the differential symbol demapper. We define the state realization of the differential decoder as

$$l_t = f(z_t \in \mathcal{X}) \in \mathcal{L} \triangleq \{0, 1, \dots, M-1\}, \quad (40)$$

where $f : \mathcal{X} \rightarrow \mathcal{L}$ maps $z_t \in \mathcal{X}$ to a specific state in \mathcal{L} . The trellis section of a DQPSK decoder is shown in Fig. 6. Note that although the state realization l_t is a mapping of the DPSK symbol z_t , the trellis input is the PSK modulated symbol x_t , which reveals the structure of the differential encoder in (32).

Using the state definitions (40) and the joint probability $p(z_t, \mathbf{y}_1^T)$ provided the IN detector, we can now rewrite (7) and express the trellis branch metric for the differential decoder as

$$\gamma_p(l_t, l_{t-1}) \triangleq p(z_t, \mathbf{y}_1^T) \cdot p_e^I(x_t), \quad (l_{t-1} \rightarrow l_t) : x_t. \quad (41)$$

where the modified branch metric uses $p(z_t, \mathbf{y}_1^T)$ as the likelihood information and uses the extrinsic prior symbol information $p_e^I(x_t)$ to denote the transition probability $p(l_t | l_{t-1})$ when the state transition $(l_{t-1} \rightarrow l_t)$ is driven by the input symbol x_t . Note that we set $p_e^I(x_t) = p(x_t) = 1/M$ in the first iteration. Using the modified branch metric (41), the joint probability of the DPSK demapper $p(l_t, l_{t-1}, \mathbf{y}_1^T)$ is derived through (4)–(11), and the joint probability of the PSK symbol is then obtained by

$$p(x_t, \mathbf{y}_1^T) = \sum_{(l_{t-1} \rightarrow l_t) : x_t} p(l_t, l_{t-1}, \mathbf{y}_1^T).$$

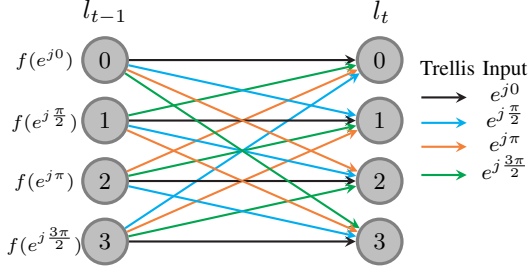


Fig. 6. Trellis section of a standalone DQPSK demapper.

TABLE I
NUMBER OF MULTIPLICATIONS FOR SEPARATE AND JOINT TURBO
RECEIVER DESIGNS WITH $M = 4$, $W = 4$, AND $L = 2$.

	$I = 0$	$I = 1$	$I = 2$	$I = 3$	$I = 10$
C_{joi}	$1024T$	$2048T$	$3072T$	$4096T$	$11264T$
C_{sep}	$1056T$	$1600T$	$2144T$	$2688T$	$6496T$

Subsequently, the iterative processing is the same as in Sec. V-B2.

D. Computational Complexity Analysis

This subsection offers a general comparison of the complexity between the joint and separate system designs. Since the main computational burden comes from the multiplication operation in the BCJR algorithm, we will concentrate on the complexity related to the number of multiplications used in the BCJR algorithm for two different realizations of the turbo systems.

Consider a length T sequence (T trellis sections) processed by a BCJR algorithm with N trellis states. For each state, it needs to consider transitions from all possible previous states, which results in a N^2 multiplication per trellis section. Therefore, the overall complexity of a BCJR operation is given by $2TN^2$, where the constant 2 accounts for the forward and backward operations. For transmission of a general cardinality M and W state Markov-Middleton channel, the super-trellis sections of the joint DPSK-IN demapper (Sec. V-B) require MW states. Considering the turbo receiver operates over I iterations, we can then write the computational complexity of the joint receiver as

$$C_{\text{joi}} = 2T \cdot (I + 1)(M^2W^2 + M^{2L}).$$

The separate design (Sec. V-C), on the other hand, requires an MW state MAP IN detector, an M state MAP DPSK demapper, and an M^L state MAP convolutional decoder. We can then write its computational complexity as

$$C_{\text{sep}} = 2T \cdot (M^2W^2 + (I + 1)(M^2 + M^{2L})).$$

In Table I, we show the computational complexity of C_{joi} and C_{sep} for a transmission of a $L = 2$ convolutional code and a DQPSK ($M = 4$) modulation over a 4-state ($W = 4$) Markov Middleton model. When operating without turbo iterations ($I = 1$), the super-trellis design in the joint system has a slightly lower complexity than a separate design. As the number of iterations increases, the computational cost of

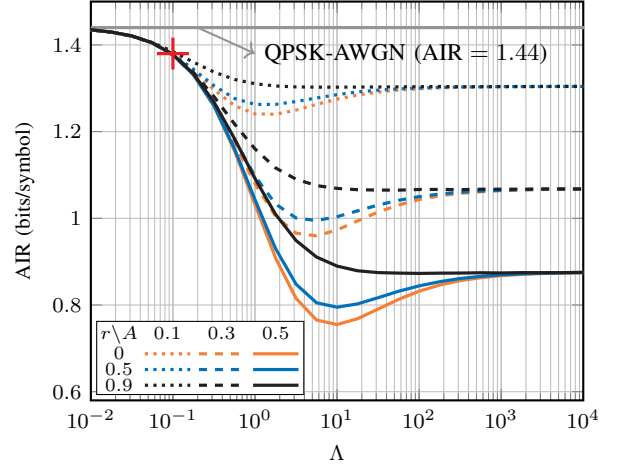


Fig. 7. AIRs versus impulsive-to-background noise ratio Λ for different impulsive index $A = 0.1, 0.3$, and 0.5 and correlation parameter $r = 0, 0.5$, and 0.9 for a QPSK modulation scheme with a 4-state Markov-Middleton impulsive noise model with SNR = 3 dB.

the joint design increases significantly and exceeds that of a separate design from the second turbo iteration. After 10 iterations, the suboptimal separate design has nearly half the computational complexity of the optimal receiver design.

VI. SIMULATION RESULTS

A. AIR Analysis

In this section, we report a detailed AIR analysis for the finite state Markov-Middleton model with a PSK transmission scheme. Specifically, we simulated 1000 independent sequences with a length of $T = 10^6$ symbols to compute the estimated AIR, where the transmitted sequence \mathbf{x}_1^T consists of QPSK ($M = 4$) modulated symbols with a symbol set \mathcal{X} following (22). The channel output sequence \mathbf{y}_1^T is obtained using (21), where the noise sequence \mathbf{n}_1^T is generated by a 4-state Markov-Middleton model with noise statistics following (16)–(18), given parameters A , Λ , r , and σ_0^2 . Note that although the mathematical derivations of this paper are in the probability domain, the actual implementation is in the log domain to prevent numerical instability. The simulated AIR with different Markov-Middleton channel parameters are shown in Fig. 7 for an SNR of 3 dB. Here, the SNR is defined as the transmitted symbol power over the background noise power

$$\text{SNR} = E\{|x_t|^2\}/\sigma_0^2.$$

To help illustrate the behavior of the AIR over impulsive-to-background noise power ratio Λ , we also plot the likelihood function for a memoryless ($r = 0$) channel with different impulsive-to-background noise power ratios ($\Lambda = 10^{-2}, 10^0, 10^4$) in Figs. 8a–8c. For simplicity, we choose a two-state (background and impulsive states) channel with impulsive index $A = 0.3$ and BPSK for the likelihood function analysis, which does not affect the generality of the presentation.

Results from Fig. 7 show that a BN-limited regime can be found when $\Lambda < 10^{-1}$ (indicated by red cross), where the

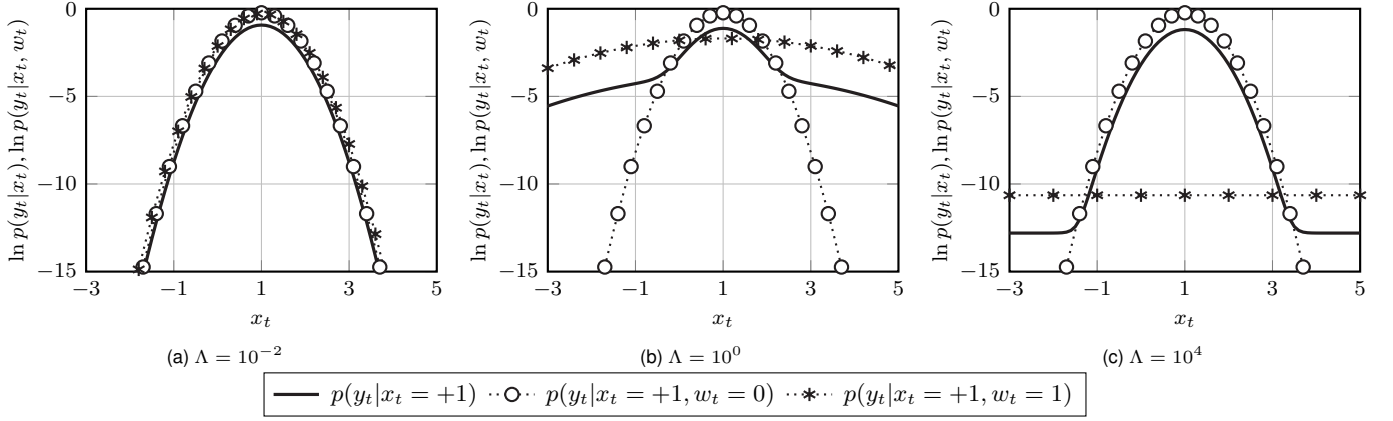


Fig. 8. The likelihood functions $p(y_t|x_t = +1)$, $p(y_t|x_t = +1, w_t = 0)$, and $p(y_t|x_t = +1, w_t = 1)$ of a 2-state memoryless ($r = 0$) Markov-Middleton model with a BPSK modulation are shown for (a) $\Lambda = 10^{-2}$ (b) $\Lambda = 10^0$ and (c) $\Lambda = 10^4$.

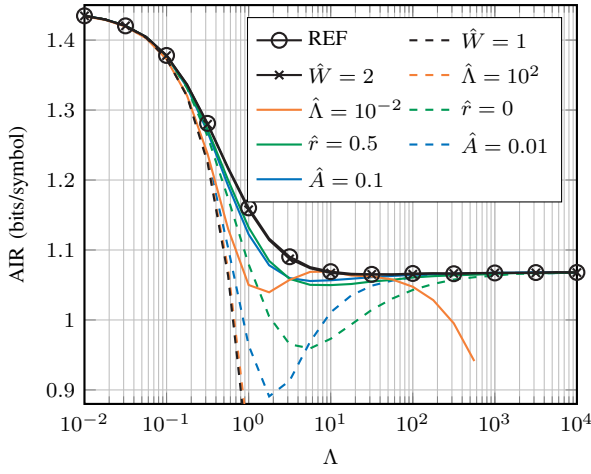


Fig. 9. AIRs versus impulsive-to-background noise ratio Λ for mismatched $\hat{A} = 0.1$ and 0.01 , $\hat{r} = 0$ and 0.5 , $\hat{\Lambda} = 10^{-2}$ and 10^2 , and $\hat{W} = 1$ and 2 , for a QPSK modulation scheme with SNR = 3 dB. The actual channel parameters are $A = 0.3$, $r = 0.9$, and $W = 4$.

noise generated by an IN state is barely distinguishable from the noise generated by a BN state ($\sigma_0^2 \approx \sigma_j^2$, $j = 1, 2, 3$) as shown in the likelihood function from Fig. 8a. In this case, the performance of the Markov-Middleton channel approaches that of the AWGN channel, with an AIR of 1.44 bits/symbol, regardless of the impulsive channel parameters A and r . From Fig. 7, we can observe that as Λ increases, the channel transitions into an IN-limited regime, where A and r become crucial in determining the AIR. A non-monotonic behavior of the AIR over Λ is shown for channels with correlation parameter $r < 0.9$ in Fig. 7, where there exist inflection points where a minimum AIR occurs. Before the inflection point, the AIR quickly worsens as Λ increases. As shown in Fig. 8b, the IN state increases the uncertainty of the overall likelihood function due to its non-negligible long tail. However, after the inflection point, the impact of the impulsive state on the overall likelihood is reduced. In particular, when $\Lambda > 10^3$, the AIR for all the channels converges to a constant value. This behavior can be explained by examining the likelihood

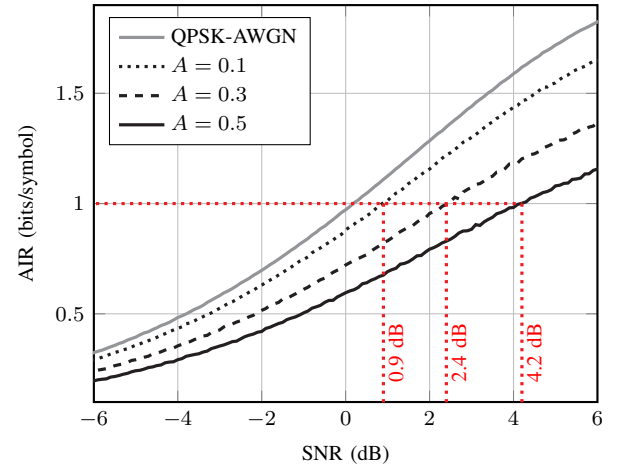


Fig. 10. AIRs versus SNR for QPSK transmission over Markov-Middleton IN channels for $A = 0.1, 0.3$, and 0.5 with fixed $\Lambda = 10$, $r = 0.9$, and $W = 4$. The solid gray line indicates the AWGN channel.

function in Fig. 8c. As the variance of the IN state increases, its likelihood function spreads, and the probability density around the mean decreases compared to that of the BN state. Consequently, the overall likelihood of transmitting a specific symbol x_t is almost entirely dominated by the BN state. It is also shown in Fig. 7 that the AIR deteriorates as the IN becomes more pronounced with increasing A . Besides, the inflection point shifts toward large Λ with a higher impulsive index A , which can be explained by (18). Specifically, when the IN samples are more active (larger A), the power of the IN must increase (larger Λ) to maintain the same noise power. On the other hand, the channel memory helps track the noise states through the transition matrix, reducing the uncertainties of the underlying IN channel and thus improving the AIR for any given value of A and Λ .

In Fig. 9, we evaluate the AIR performance under mismatched decoding scenarios where imperfect channel knowledge exists. In all simulations, we assume that the Markov-Middleton channel is characterized by parameters $A = 0.3$, $r = 0.9$, and $W = 4$. This setup corresponds to a highly cor-

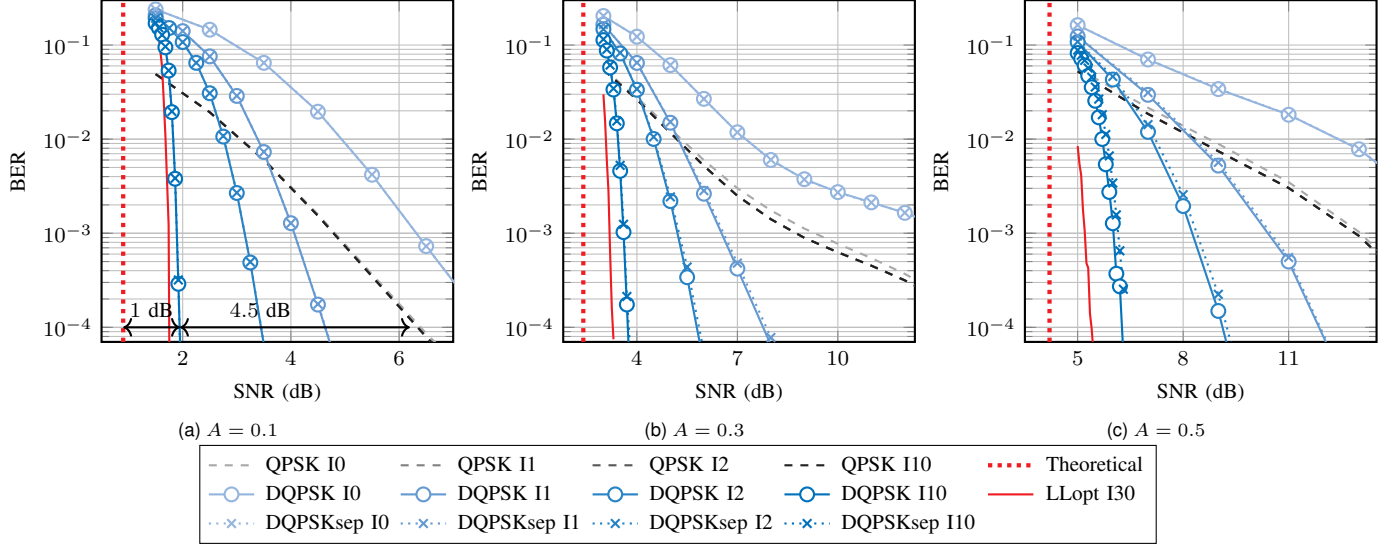


Fig. 11. BER performance over iterations for QPSK-IN (dashed lines), turbo-DQPSK-IN (circle solid lines), and suboptimal turbo-DQPSK-IN designs (cross dotted lines) over the Markov-Middleton channel with impulsive index (a) $A = 0.1$ (b) $A = 0.3$ and (c) $A = 0.5$, where $W = 4$, $\Lambda = 10$ and $r = 0.9$ are fixed for all simulations. The dotted red vertical lines indicate the simulated theoretical bound derived in Fig. 10. The solid red lines indicate the ultimate performance bound of the proposed turbo-DPSK-IN receiver with perfect CSI. All simulations have an interleaver depth of 100000 bits.

related, bursty IN environment, which is commonly observed in practice [4], [6]. We first examine the extreme cases by assuming $\hat{W} = 1$ (black dashed line) and $\hat{\Lambda} = 10^{-2}$ (orange dashed line). This simplification effectively reduces the receiver to an AWGN detector. While they perform adequately in the BN-limited regime ($\Lambda < 10^{-1}$), their performance severely deteriorates as the true channel transitions into the IN-limited regime ($\Lambda > 10^{-1}$). Additionally, ignoring channel memory by assuming $r = 0$ (green dashed line) leads to a memoryless receiver design. This simplification results in an AIR loss of up to 0.1 bits/symbol compared to the memory-aware receiver under highly correlated impulsive conditions, a finding that aligns with previous observations in [18]. This highlights the need for memory-aware detection schemes or alternative techniques, such as orthogonal frequency division multiplexing (OFDM) approaches, to mitigate the impact of temporally correlated channels. Moreover, a mismatch in the impulsive parameters A and Λ imposes a notable performance loss, emphasizing the importance of accurate channel estimation in practical systems. On the other hand, the receiver is relatively robust to state mismatch: assuming a simple 2-state model (crosses) yields similar AIR performance to the true 4-state model. This suggests that the complexity of the receiver can be reduced without substantial performance loss as long as the key statistical properties of the IN are adequately captured.

As a reference for our practical receiver design, we present the AIR as a function of SNR in Fig. 10. Specifically, the SNR required to achieve a target AIR of 1 bits per transmitted DQPSK symbol, which corresponds to a half-rate encoder, is 0.9 dB, 2.4 dB, and 4.2 dB for impulsive index $A = 0.1$, 0.3, and 0.5, respectively. These performance bounds will be used to benchmark our turbo-DPSK-IN receiver designs in the following subsection.

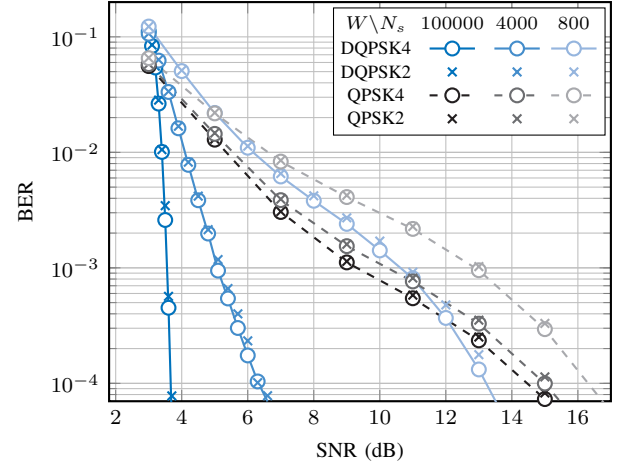


Fig. 12. BER performance for practical receiver design considerations with underestimated channel state $W = 2$ and limited interleaver depths of 100000, 4000, and 800, respectively, for the proposed suboptimal turbo-DQPSK receiver after 10 iterations. The IN channel is characterized by $W = 4$, $A = 0.3$, $\Lambda = 10$, and $r = 0.9$.

B. Proposed Turbo-DPSK-IN Receiver Performance

This section reports the numerically simulated bit error rate (BER) performance of the proposed optimal and suboptimal turbo-DPSK-IN receivers under a 4-state Markov-Middleton IN channel. A standard half-rate convolutional code with generators $(5, 7)_8$ was used. The number of information bits per data frame is 50000, which leads to a bit interleaver with a 100000 bits depth. Such a large interleaver size not only increases the iterative decoding capability but also disperses the bursty impulse noise, which is crucial for the system performance, especially in highly correlated ($r > 0.9$) channels. A QPSK modulation is employed to map the interleaved coded

bits to symbols, after which a differential modulator processes the symbols as in (32). Finally, the differentially modulated symbols are transmitted through a Markov-Middleton channel, where the observed sequence \mathbf{y}_1^T is generated following (33). For conventional QPSK transmission, the observation is made via (21).

Figs. 11a–11c show the BER performance of the proposed joint turbo-DPSK-IN receiver (solid lines) with respect to the number of iterations for different impulsive index $A = 0.1, 0.3$, and 0.5 . When comparing to the performance of the conventional PSK-IN receiver (dashed lines), we observe that the turbo-DPSK-IN receiver significantly outperforms the PSK-IN receiver in all cases after the first turbo iteration, with a performance gain of around 4.5 dB at a BER of 10^{-4} for $A = 0.1$. The performance gain is more pronounced for larger impulsive index A . This demonstrates the effectiveness of incorporating a rate-one differential decoder into the turbo receiver. After 10 turbo iterations, the proposed turbo receiver has about 1.1, 1.4, and 2.1 dB SNR gaps compared to the theoretical bounds derived in Fig. 10 for channel characterized by $A = 0.1, 0.3$, and 0.5 , respectively. The performance gap is larger for a more severe IN channel, which is expected as the channel becomes more challenging to handle. Note that the computation complexity for the joint IN detector is the same for both joint turbo-DPSK-IN and PSK-IN receivers, as the rate-one differential structure is efficiently combined into the trellis structure without increasing the number of states as shown in Figs. 3a and 3b.

The performance of the joint turbo-DPSK-IN receiver is also compared to its suboptimal separate design (dotted cross lines in Figs. 11a–11c), where the turbo decoder and the IN detector (equalizer) are designed separately. The separate design is implemented by using the same MAP equalizer as in [19], [23], which only computes the posterior symbol probability once without iterative updates. The results show that the suboptimal separate design can approximate closely to the optimal joint design without much degradation, especially in a mild IN channel (Fig. 11a). Such observation was also identified in [18]. This finding suggests that the use of a suboptimal design is preferable as it has only around half the complexity of the optimal design for an iteration number of 10. However, in a severely activated IN channel (Fig. 11c), the separate design shows a performance loss of around 0.2 dB compared to the joint design, which is expected to increase with a larger impulsive index A .

To gauge the ultimate performance of our proposed turbo-DPSK-IN scheme under the Markov-Middleton channel, we simulate the performance of the proposed turbo-DPSK-IN receiver with perfect channel state information (CSI) at the receiver. This is achieved by assuming that the noise state realization is perfectly known at the receiver, which allows for a perfect equalization of the received signal. The results are shown in Figs. 11a–11c as solid red lines. The perfect CSI simulation serves as a benchmark for the performance of our proposed turbo system, where we assume that a large number of iterations (30 iterations) are performed. The results show that the ultimate performance of the proposed turbo-DPSK-IN system is around 1 dB away from the theoretical bounds,

regardless of channel conditions. For $A = 0.1$, a turbo-DPSK-IN receiver with 10 iterations is already close to the ultimate performance, while for $A = 0.5$, more iterations are required to achieve the best possible result.

In Fig. 12, we evaluate the performance of the separate receiver design in a setting with limited interleaver depth and mismatched channel states. The results are shown for a fixed 4-state Markov Middleton model with $A = 0.3$, $r = 0.9$, and $\Lambda = 10$. The number of turbo iterations is set to 10. We first design a receiver that only assumes $\hat{W} = 2$, which leads to a total of $2M = 8$ trellis states in the IN detector. In this case, the receiver is designed to ignore the higher impulsive noise states. The results show that the performance of the receiver with a mismatched $\hat{W} = 2$ state assumption is very close to that of the matched receiver design with $W = 4$ states, which is also identified in Fig. 9. This is an important observation as we can design an efficient receiver with a reduced number of states without much performance loss. The results of Fig. 12 also show that the receiver is sensitive to the interleaver depth. A smaller interleaver depth of 4000 leads to a performance loss of around 2.7 dB, while a depth of 800 results in significant performance degradation of around 10 dB loss at a BER of 10^{-4} for the turbo-DPSK-IN system. The benefits of using a large interleaver depth are mainly twofold. First, it improves the MAP-based IN detector (equalizer) performance, and second, it effectively spreads the decoding errors for the two constituent decoders, which is crucial for the turbo decoding performance. We can see that the conventional PSK-IN (black dashed lines) can only acquire the detector-related benefits, while the proposed turbo-DPSK-IN system (blue solid lines) can benefit from both. This is because the turbo-DPSK-IN system can effectively spread the decoding errors thanks to the recursive nature of the differential decoder, which is crucial for turbo decoding performance.

VII. CONCLUSIONS

In this paper, we proposed robust turbo receiver structures that can effectively mitigate the impact of bursty impulses, modeled by a 4-state Markov-Middleton model, by incorporating a rate-one differential decoder into the receiver design. We started by investigating the AIR between the PSK-modulated symbols and the channel output sequence for various channel conditions. We found that the impulsive index significantly influences the AIR. Also, we observed a non-monotonic relationship between the estimated AIR and the impulsive-to-background noise power ratio, which can be further explained by evaluating the likelihood function for the BN and IN states. Furthermore, channel memory reduces the uncertainty of the given IN channel, thereby increasing the AIR. Mismatched decoding scenarios are also considered in the AIR analysis. In the second part of the paper, we carefully derive the proposed turbo-DPSK-IN receiver design, which incorporates a differential decoder into the MAP-based IN detector. Results show that the proposed turbo-DPSK-IN receiver significantly outperforms the conventional MAP-based PSK-IN receiver by more than 4.5 dB with an ultimate performance gap of around 1 dB from the AIR-derived performance bound. Additionally,

we proposed a suboptimal separate receiver design, which only has half the complexity of the joint design but still sufficiently approximates the optimal joint receiver design. The proposed receiver design is also shown to be robust against the underestimated IN-state scenario.

This paper shows that a simple rate-one differential code can effectively improve the receiver performance under the serially concatenated turbo structure in the presence of bursty IN. Although the focus and derivation of this paper are based on convolutional codes, the proposed system can be straightforwardly adapted to other coding schemes.

ACKNOWLEDGMENTS

This work was funded by the RAISE collaboration framework between Eindhoven University of Technology and NXP, including a PPS-supplement from the Dutch Ministry of Economic Affairs and Climate Policy.

REFERENCES

- [1] A. Maouloud, M. Klingler and P. Besnier, "A test setup to assess the impact of EMI produced by on-board electronics on the quality of radio reception in vehicles," *IEEE Trans. Electromagn. Compat.*, vol. 63, no. 6, pp. 1844–1855, Dec. 2021.
- [2] X. Gao, D. Su and Y. Li, "Study on electromagnetic interference of DC/DC converter used in the EV," *Asia-Pacific Symposium on Electromagnetic Compatibility (APEMC)*, pp. 258–261, 2015.
- [3] K. Pliakostathis, "Research on EMI from modern electric vehicles and their recharging systems," *International Symposium on Electromagnetic Compatibility (EMC)*, pp. 1–6, 2020.
- [4] C.-H. Chen, W.-H. Huang, B. Karanov, Y. Wu, A. Young, W. van Houtum, "Analysis of impulsive interference in digital audio broadcasting systems in electric vehicles," *Symposium on Information Theory and Signal Processing in the Benelux (SITB)*, 2024.
- [5] Q. Shan et al., "Noise amplitude distribution of impulsive noise from measurements in a power substation," *International Universities Power Engineering Conference (UPEC)*, pp. 1–5, 2009.
- [6] F. Sacuto, F. Labeau and B. L. Agba, "Wide band time-correlated model for wireless communications under impulsive noise within power substation," *IEEE Trans. Wireless Commun.*, vol. 13, no. 3, pp. 1449–1461, Mar. 2014.
- [7] R. Pighi, M. Franceschini, G. Ferrari and R. Raheli, "Fundamental performance limits for PLC systems impaired by impulse noise," *IEEE International Symposium on Power Line Communications and Its Applications (ISPLC)*, pp. 277–282, 2006.
- [8] M. Zimmermann and K. Dostert, "Analysis and modeling of impulsive noise in broad-band powerline communications," *IEEE Trans. Electromagn. Compat.*, vol. 44, no. 1, pp. 249–258, Feb. 2002.
- [9] W. van Houtum, "Time-division spatial interference rejection (TDSIR)-procedure," U.S. Patent 11,722,197B2, 2022.
- [10] I. Landa, M. M. Vélez, A. Arrinda, R. Torre and M. Fernández, "Impulsive noise characterization and its effect on digital audio quality," *IEEE International Symposium on Broadband Multimedia Systems and Broadcasting (BMSB)*, pp. 1–3, 2015.
- [11] Q. Shan et al., "Estimation of impulsive noise in an electricity substation," *IEEE Trans. Electromagn. Compat.*, vol. 53, no. 3, pp. 653–663, Aug. 2011.
- [12] S. A. Bhatti, I. A. Glover, R. Atkinson, Q. Shan, Y. Yang, J. M. R. S. Neto, "Vulnerability of bluetooth to impulsive noise in electricity transmission substations," *IET International Conference on Wireless Sensor Network (WSN)*, pp. 53–58, 2010.
- [13] N. B. Sarr, A. K. Yazbek, H. Boeglen, J. P. Cances, R. Vauzelle and F. Gagnon, "An impulsive noise resistant physical layer for smart grid communications," *IEEE International Conference on Communications (ICC)*, pp. 1–7, 2017.
- [14] G. Ndo, P. Siohan and M. -H. Hamon, "Adaptive Noise Mitigation in Impulsive Environment: Application to Power-Line Communications," *IEEE Trans. Power Deliv.*, vol. 25, no. 2, pp. 647–656, Apr. 2010.
- [15] H. Oh and H. Nam, "Design and Performance Analysis of Nonlinearity Preprocessors in an Impulsive Noise Environment," *IEEE Trans. Veh. Technol.*, vol. 66, no. 1, pp. 364–376, Jan. 2017.
- [16] D. Middleton, "Statistical-physical model of electromagnetic interference," *IEEE Trans. Electromagn. Compat.*, vol. EMC-19, no. 3, pt. 1, pp. 106–127, Aug. 1977.
- [17] D. Middleton, "Non-Gaussian noise models in signal processing for telecommunications: new methods and results for class A and class B noise models," *IEEE Trans. Inf. Theory*, vol. 45, no. 4, pp. 1129–1149, May 1999.
- [18] D. Fertonani and G. Colavolpe, "On reliable communications over channels impaired by bursty impulse noise," *IEEE Trans. Commun.*, vol. 57, no. 7, pp. 2024–2030, Jul. 2009.
- [19] G. Ndo, F. Labeau and M. Kassouf, "A Markov-Middleton model for bursty impulsive noise: Modeling and receiver design," *IEEE Trans. Power Deliv.*, vol. 28, no. 4, pp. 2317–2325, Oct. 2013.
- [20] D. Fertonani and G. Colavolpe, "Theoretical limits and practical detection schemes for channels affected by class-A impulse noise," *IEEE Global Telecommunications Conference (GLOBECOM)*, pp. 146–150, 2007.
- [21] D. Fertonani and G. Colavolpe, "A robust metric for soft-output detection in the presence of class-A noise," *IEEE Trans. Commun.*, vol. 57, no. 1, pp. 36–40, Jan. 2009.
- [22] R. Haring and A. J. Han Vinck, "Performance bounds for optimum and suboptimum reception under Class-A impulsive noise," *IEEE Trans. Commun.*, vol. 50, no. 7, pp. 1130–1136, Jul. 2002.
- [23] M. S. Alam, B. Selim, G. Kaddoum and B. L. Agba, "Mitigation techniques for impulsive noise with memory modeled by a two state Markov-Gaussian process," *IEEE Syst. J.*, vol. 14, no. 3, pp. 4079–4088, Sep. 2020.
- [24] H. Nakagawa, D. Umehara, S. Denno and Y. Morihoro, "A decoding for low density parity check codes over impulsive noise channels," *International Symposium on Power Line Communications and Its Applications (ISPLC)*, pp. 85–89, 2005.
- [25] J. Mitra and L. Lampe, "Convolutionally coded transmission over Markov-Gaussian channels: analysis and decoding metrics," *IEEE Trans. Commun.*, vol. 58, no. 7, pp. 1939–1949, Jul. 2010.
- [26] F. G. Mengistu, D. -F. Tseng, Y. S. Han, M. A. Mulatu and L.-C. Chang, "A Robust decoding scheme for convolutionally coded transmission through a Markov Gaussian channel," *IEEE Trans. Veh. Technol.*, vol. 63, no. 9, pp. 4344–4356, Nov. 2014.
- [27] D.-F. Tseng, F. G. Mengistu, Y. S. Han, M. Abera Mulatu, L.-C. Chang and T. -R. Tsai, "Robust turbo decoding in a Markov Gaussian channel," *IEEE Wireless Commun. Lett.*, vol. 3, no. 6, pp. 633–636, Dec. 2014.
- [28] D. Umehara, H. Yamaguchi and Y. Morihoro, "Turbo decoding in impulsive noise environment," *IEEE Global Telecommunications Conference (GLOBECOM)*, pp. 194–198, 2004.
- [29] G. Colavolpe, "Classical coherent receivers for differentially encoded M-PSK are optimal," *IEEE Commun. Lett.*, vol. 8, no. 4, pp. 211–213, Apr. 2004.
- [30] K. R. Narayanan and G. L. Stuber, "A serial concatenation approach to iterative demodulation and decoding," *IEEE Trans. Commun.*, vol. 47, no. 7, pp. 956–961, Jul. 1999.
- [31] P. Hoeher and J. Lodge, "Turbo DPSK: iterative differential PSK demodulation and channel decoding," *IEEE Trans. Commun.*, vol. 47, no. 6, pp. 837–843, Jun. 1999.
- [32] W. van Houtum, "Two-dimensional block-based reception for differentially encoded OFDM systems: A study on improved reception techniques for digital audio broadcasting systems," Ph.D. dissertation, Dept. Elect. Eng., Technische Universiteit Eindhoven, Eindhoven, Netherlands, 2012.
- [33] I. Lee, "The effect of a precoder on serially concatenated coding systems with an ISI channel," *IEEE Trans. Commun.*, vol. 49, no. 7, pp. 1168–1175, Jul. 2001.
- [34] D. M. Arnold, H.-A. Loeliger, P. O. Vontobel, A. Kavcic and W. Zeng, "Simulation-based computation of information rates for channels with memory," *IEEE Trans. Inform. Theory*, vol. 52, no. 8, pp. 3498–3508, Aug. 2006.
- [35] L. R. Bahl, J. Cocke, F. Jelinek, and J. Raviv, "Optimal decoding of linear codes for minimizing symbol error rate," *IEEE Trans. Inform. Theory*, vol. 20, no. 2, pp. 284–287, Mar. 1974.